Environ. Sci. Technol. 1997, 31, 2634–2641

Horizontal Bubble Train Apparatus for Heterogeneous Chemistry Studies: Uptake of Gas-Phase Formaldehyde

E. SWARTZ, J. BONIFACE, I. TCHERTKOV, O. V. RATTIGAN, D. V. ROBINSON, AND P. DAVIDOVITS*

Department of Chemistry, Merkert Chemistry Center, Boston College, Chestnut Hill, Massachusetts 02167

D. R. WORSNOP, J. T. JAYNE, AND C. E. KOLB

Center for Chemical and Environmental Physics, Aerodyne Research, Inc., Billerica, Massachusetts 01821

A new horizontal bubble train apparatus has been built to conduct time-resolved gas–liquid interaction studies of interest in atmospheric chemistry. In the apparatus, liquid is pumped horizontally through a 0.4 cm i.d. quartz tube at a controlled speed of 15–35 cm/s. A low-pressure (about 50 Torr) gas flow, carrying the trace gas of interest diluted in helium carrier gas, is injected through a moveable injector into the liquid flow forming well-defined bubbles that fill the diameter of the tube. In a controlled way, 10–25 bubbles are formed per second. The outlet gas flow is then sampled by a differentially pumped mass spectrometer. The position of the bubble injector, which is computer controlled by a stepping motor, determines the bubble travel distance and therefore the gas-liquid interaction time (typically 0.1–10 s). Modeling of the gas uptake and the validation of the apparatus performance are described. The apparatus can measure Henry's law coefficients (H) for non-reactive species in the range 10^{-3} to 3.0 M atm^{-1}. For reactive species (first-order reaction rate k), the apparatus measures $Hk^{1/2}$ values in the range 0.04–150 (M atm^{-1} s$^{-1/2}$). If the Henry's law coefficient of a species is known, then first order reaction rates in the range 1–10^8 s^{-1} can be measured. Using this bubble train apparatus, the uptake of gas phase formaldehyde as a function of pH (0–11) and NaCl concentration (0–4 M) has been measured. The Setchenow coefficient for formaldehyde in NaCl solution at 293 K has been determined to be $K_s = 0.072 \pm 0.004$ M^{-1}.

Introduction

Heterogeneous gas–liquid interactions involving aqueous droplets and aerosols in clouds and fogs have been recognized as major mechanisms for the chemical transformations both in the troposphere and in the stratosphere (see, for example, refs 1–14). The atmospheric importance of heterogeneous interactions has led to the development of several laboratory techniques to study such processes. Among the most widely used techniques are the entrained aerosol flow tube (*15*, *16*), Knudsen cell reactor (*17*), coated wall flow tube (*18*), and the droplet train flow tube (*19–21*). Each of these techniques has a range of applicability, with particular advantages and limitations. (For a review of these and other techniques, see ref 22). Recently, we began to experiment with bubbles as the medium for the study of heterogeneous gas–liquid interactions.

In a laboratory experiment designed to study heterogeneous interactions, the uptake of the trace gas of interest is measured and can be expressed in terms of an uptake coefficient, γ_{meas}, defined as

$$\gamma_{meas} = \frac{\text{no. of molecules lost to the surface (molecules s}^{-1})}{\text{no. of gas–surface collisions (collisions s}^{-1})} \quad (1)$$

The experimentally measured uptake coefficient (γ_{meas}) is a function of the mass accommodation coefficient, gas and liquid phase diffusion, Henry's law saturation, gas–surface interaction time, and in some cases liquid and surface chemistry. The challenge is to design experiments in which these effects can be separated.

With bubbles as the medium of interaction, rates of heterogeneous processes corresponding to small uptake coefficients in the range 10^{-4}–10^{-7} can be measured (*23*, *24*). This technique complements the droplet train flow tube apparatus that has been used extensively in our laboratory to measure relatively large gas uptakes ($\gamma_{meas} > 5 \times 10^{-4}$). The primary difference between the bubble train and droplet experiments lies in the gas–liquid interaction times: $t = 0.1$–10 s for bubbles and 3–20 ms for droplets. The longer interaction time in the bubble train increases the number of gas–liquid collisions and, thus, the sensitivity to small gas uptake rates.

While bubblers have been employed to promote gas–liquid interactions since the inception of the field of chemistry, until recently they have not been used to conduct quantitative time-resolved studies. The basic task in building a bubble apparatus suitable for quantitative studies is to characterize the device and to accurately model the uptake. The device characterization involves an accurate determination of the bubble size, shape, and interaction time within the liquid. The modeling has to take into account the nature of the liquid flow, which involves expressing the uptake as a function of several parameters obtained by fitting the model to the experimental data. The uptake rates, for the species studied in the bubble train apparatus, are relatively slow so that gas-phase diffusive transport need to be considered for only the very fastest uptake rates. Mass accommodation does not limit the uptake in the range of this apparatus. Throughout the region of reliable operation, the uptake of the trace gas in the bubble is governed by Henry's law coefficient (H) and/or the interfacial or bulk phase reaction rate (k) for the species. The model is calibrated by studying species with known H and k. The bubble train apparatus provides the possibility of detecting the effect on the uptake of reactions at the gas–liquid interface.

Our first bubble apparatus utilized a vertical column of bubbles rising through the liquid (*23*). A low-pressure gas flow, containing trace gas diluted in helium carrier gas, was bubbled through a flask containing about 4 L of liquid. The outlet gas flow was then sampled by a differentially pumped mass spectrometer. Using this apparatus, we were able to conduct selected kinetics studies, and we measured Henry's law constants and Setchenow coefficients for the biogenic reduced sulfur species DMS, H_2S, CS_2, CH_3SH, and OCS (*24*).

There are certain inherent limitations associated with the vertical bubble column apparatus. Since the bubbles rise vertically through the liquid, driven by buoyancy, the velocity, shape, and trajectory of the bubbles are not fully controlled. The depth from which the bubbles can be injected is limited,

S0013-936X(97)00042-4 CCC: $14.00

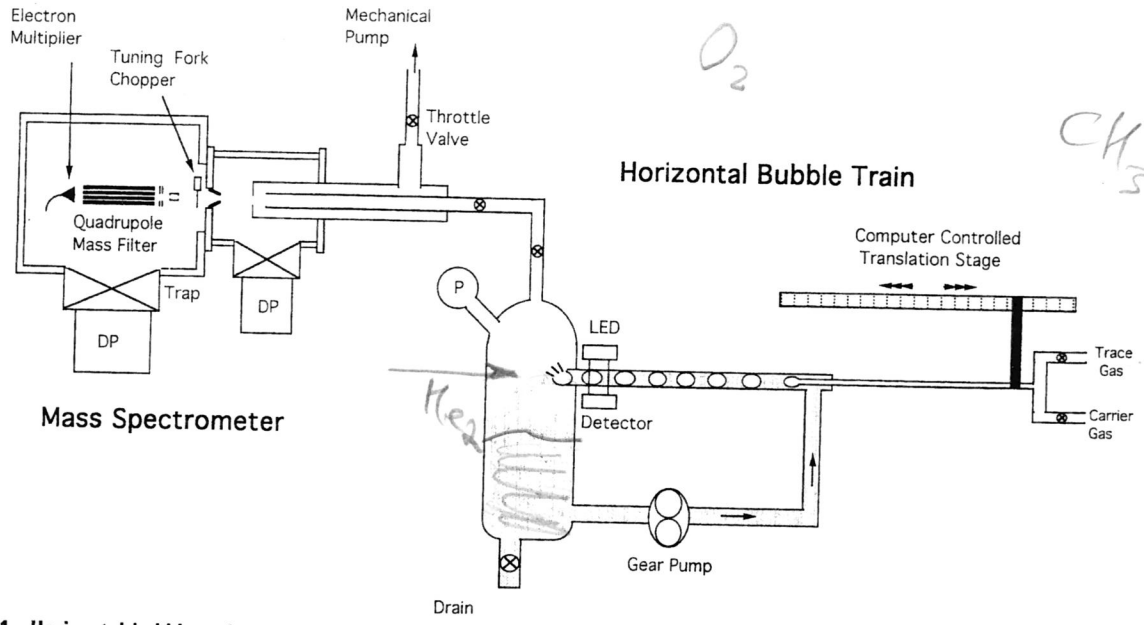

FIGURE 1. Horizontal bubble train apparatus.

and therefore the gas interaction time is circumscribed to times less than about 0.5 second. Of necessity, there is always a significant thickness of liquid between the wall and the gas in the bubble, which hinders photochemical experiments in which the gas–liquid interface is illuminated by light simulating solar radiation. We have now completed the development of a new bubble train apparatus in which the bubbles move horizontally carried through a tube by a flowing liquid. The new configuration is a significant improvement over the vertical bubble column apparatus overcoming the limitations noted above. In this paper, we describe the operation and calibration of this horizontal bubble train apparatus, and we present uptake data for formaldehyde obtained with this technique.

Formaldehyde is an important trace gas in the atmosphere (*4*) emitted by combustion exhaust sources (*25*) as well as many building materials and furnishings (*26*). It is a key reactive intermediate in the photochemical oxidation of airborne hydrocarbons and serves as one of the most potent gas-phase precursors of ozone pollution in urban and industrialized regions (*27*). Gas–liquid interactions with cloud droplets and aerosols remove atmospheric CH_2O from the gas phase resulting in significant levels of formaldehyde in rain, snow, and fog (*28*). In fog and cloud droplets, CH_2O participates in several atmospherically important reactions (*29, 30*). In this study, the uptake of formaldehyde was measured as a function of pH and NaCl concentration. The results were used in part to calibrate the apparatus and also to extend the range of previous droplet uptake studies (*31, 32*). The uptake measurements as a function NaCl concentration were used to obtain the Setchenow coefficient for formaldehyde in NaCl solutions.

Experimental Considerations

Description of the Horizontal Bubble Train Apparatus. A schematic of the apparatus is shown in Figure 1. Liquid is pumped through the 0.4 cm i.d. quartz tube at a controlled speed of 15–35 cm/s. The system is designed to operate with aqueous solutions as well as with concentrated sulfuric acid. The liquid is temperature controlled by a coolant flowing through a glass jacket surrounding the reservoir flask. A low-pressure (about 50 Torr) gas flow, carrying trace gas of interest diluted in helium carrier gas, is injected into the liquid flow via 1/12 in. (14 gauge) stainless steel tubing. Well-defined bubbles are formed filling the diameter of the tube. The bubbles are non-spherical with length between 0.4 and 1.2 cm depending on the gas and liquid flow conditions. Ten to 25 bubbles are formed per second at a controlled rate. The liquid flow carries the bubbles to the end of the flow tube. A curved trough positioned at the end of the flow tube promotes a smooth flow of the exiting liquid into the reservoir and the separation of the entrained gas from the liquid. The separation of the gas from the liquid proceeds most smoothly with the injector tip bent upwards in the direction opposite to the trough.

After the bubble breaks at the end of the flow tube, the subsequent interaction time of the gas with the reservoir liquid surface must be minimized. This is accomplished by means of a gas inlet (not shown in Figure 1) positioned coaxially to the flow tube, which carries a flow of helium and water vapor about 50 times greater than the flow containing the trace gas. This coaxial flow is centered on the bubble breaking region and dilutes the trace gas. The dilution and entrainment rapidly remove the trace gas from the "wet" environment, minimizing unwanted heterogeneous interactions above the liquid reservoir. The trace species is then sampled by a differentially pumped mass spectrometer. Other methods of gas species detection can be easily coupled to the apparatus. To avoid condensation of less volatile trace species, provisions have been made to heat the passageway between the reservoir and the mass spectrometer.

The position of the bubble injector that is computer controlled by a stepping motor determines the bubble travel distance and therefore the gas–liquid interaction time. The frequency, size, and speed are monitored in the apparatus by two light-emitting diodes (LED) positioned along the flow tube and separated by a fixed distance of 2 cm (see Figure 1).

Experimental Procedure. An experimental run begins with the bubble injector positioned outside the flow tube, out of contact with the flowing liquid. At this point the gas flows through the injector without interaction with the liquid surface. The computer-controlled translation stage then starts a 134 cm withdrawal of the injector into the flow tube. The first centimeter of the translation is outside the liquid. Bubbles are formed as the injector enters the liquid. Once formed, the bubble, which contains the trace and carrier gases, becomes saturated with water vapor. The coaxial H_2O/He purge flow described earlier also provides a steady equilibrium-determined source of water vapor in the region above the liquid reservoir, thus minimizing the pressure/flow change when the bubble exits the flow tube. The auxiliary coaxial

Flow

FIGURE 2. Stroboscopic photograph of bubbles. Inside diameter of the tube is 0.4 cm.

gas flow has been varied to ascertain that it does not affect the uptake measurements.

Specifics of the Experiment. We note that there are two time scales associated with this experiment. First is the travel time of the gas bubble from the injector orifice to the end of the tube. This sets the gas–liquid interaction time, which varies from 0.1 to about 10 s. The other is the travel time of the injector into the flow tube. Under our experimental conditions, the full 134 cm withdrawal into the flow tube takes about 360 s. The withdrawal speed must be slow enough so that the gas uptake at any injector position is independent of the injector speed.

The computer-controlled stepping motor (Velmex Inc.) has a linear speed ranging from 0 to 2 cm/s. In our experiments, the translation stage is operated at an initial speed of 0.033 cm/s and slowly accelerates to a final speed of 0.4 cm/s over the course of the 134 cm of the bubble injector travel. During the travel time, the mass spectrometer signal is sampled at a rate of 25 Hz. The slower injector speed at the beginning of the run results in sampling proportional to the amount of information contained in the uptake data. The acquired data are averaged and saved at intervals of 3 s, which correspond to an injector travel of 0.1 cm at the start of the run and 1.2 cm toward the end of the run. The pressure is monitored at the same rate. In order to maintain smooth flows, the total pressure above the liquid reservoir is maintained at 30 Torr above the water vapor pressure.

Absolute trace gas density in the bubbles is determined by producing bubbles with calibrated flows of trace and carrier gases. The entry of water vapor into the bubble is accounted for by using a dilution factor that is determined by a series of measurements with noble gases to calibrate the effect of dilution at the mass spectrometer. Gas flows are measured with a mass flow meter (Matheson 8100 Series). The liquid flow is measured using a calibrated rotameter (Matheson 601 Series). The following flows were used in the experiment: Helium carrier gas flow for the formation of the bubble and trace gas entrainment was 0.05 standard mL/s. The coaxial He purge flow was 3 standard mL/s. The liquid flow rate was in the region 1–3 mL/s. The trace gas density inside the bubble was varied from 5×10^{14} to 5×10^{16} cm^{-3}.

Characterization of Bubbles. The formation of vertically rising bubbles at submerged orifices is well documented in the literature (*33–37*). However, to our knowledge, the formation of bubbles in a horizontal flow tube apparatus such as ours has not been previously studied. Well-defined regular bubbles can in fact be formed in such a system. The formation of a bubble is due to the interplay of the gas and liquid flows. When the gas pressure in the injector tip is a few Torr above the internal pressure of the liquid, gas emerges from the tip in the direction of liquid flow. The emerging gas bubble fills part of the tube, impeding the flow of liquid. As a result, the liquid pressure upstream of the bubble rises until it becomes high enough to detach the bubble from the injector tip. The detached bubble is carried downstream, and a new bubble begins to form at the injector. Well-formed bubbles are produced at moderate gas flow rates of approximately 0.05 standard mL/s and liquid flow rates of 1–3 mL/s. A train of such bubbles is shown in Figure 2. The photograph was made with stroboscopic illumination, which provides an independent check on bubble velocity.

To model the gas uptake into the liquid, the following parameters must be known: surface area, volume and speed of the bubble, and volume of the liquid between bubbles. Photographic studies show that fully evolved bubbles are bullet-shaped. The front section of the bubble is well approximated by an ellipse. The center section is the shape of a cylinder, and the rear of the bubble is approximated by the arc of a sphere. The passage of the bubble through the light of the LEDs generates pulses in the detected light that are monitored by computer and provide a direct measure of bubble length and frequency yielding the velocity of the bubble.

Modeling the Gas Uptake

A key task in the development of the bubble apparatus into a quantitative tool has been the proper modeling of the gas uptake and the validation of the apparatus performance. Gas uptake in the horizontal bubble train experiment is governed by the same physical processes that govern the gas uptake in the earlier vertical bubble column device (*23*). However, in modeling gas uptake in the new apparatus, we have taken a simpler approach.

As stated in the Introduction, the measured uptake is a function of the mass accommodation coefficient, gas and liquid phase diffusion, Henry's law saturation, gas–surface interaction time, and, in the case of reactive species, also liquid and surface chemistry (*22*). Danckwerts (*38*) solved the uptake equations analytically for the case where the species in the gas phase is not substantially depleted. Since the uptake coefficient of the species studied in the bubble apparatus is small, mass accommodation does not limit the uptake. In the initial formulation, gas-phase diffusion is also neglected. However, in the regions of the fastest uptake, limitations due to gas-phase transport are noted and are taken into account.

When mass accommodation and gas-phase transport do not limit gas uptake, then the trace gas is near saturation, and the trace gas uptake flux is determined by the rate at which the species is diffusively transported away from the interface. This transport rate depends on the liquid-phase diffusion coefficient D_l and on the concentration gradient of the species. Liquid-phase irreversible reaction of the solvated trace species steepens the concentration gradient by additional removal of the species from the mass transport profile, which results in an enhanced uptake rate. Therefore, the uptake rate is also a function of the pseudo-first-order irreversible reaction rate (k) of the solvated trace species of interest. In these limits, Dankwerts' expression for the flux (J) of gas molecules into a semi-infinite liquid is

$$J = n_g HRT[(D_l/\pi t)^{1/2} \exp(-kt) + (D_l k)^{1/2} \operatorname{erf}(kt)^{1/2}] \quad (2)$$

Here n_g is the gas-phase density of the trace species, R is the gas constant, T is the temperature, t is the gas–liquid contact time, and H is the Henry's law constant (in M/atm).

Although both bracketed terms in eq 2 contain the reaction rate k, their effects can be distinguished. The first term represents principally the effect of liquid-phase solubility on the uptake. The second term represents mainly the effect of irreversible reaction of the species in the liquid. We note that in the absence of chemical reaction ($k = 0$), the flux tends toward zero as the gas–liquid contact time increases and the liquid reaches saturation. At equilibrium, the liquid is saturated and the density of the solvated species n_l is $n_l = n_g HRT$. Under saturated conditions, the number of molecules leaving and entering the liquid is the same, and the net flux is zero. Chemical reaction causes a continued removal of solvated species, which prevents the attainment of equilibrium and therefore maintains a flux of species into the liquid.

The amount of gas Q that enters the liquid per cm^2 during a time period τ is obtained by integrating the flux J from $t =$

0 to τ. Such an integration yields

$$Q = n_g HRT[(\tau D_l/\pi)^{1/2} \exp(-k\tau) + \{\tau(D_l k)^{1/2} + 1/2(D_l/k)^{1/2}\} \operatorname{erf}(k\tau)^{1/2}] \quad (3)$$

The gas uptake is modeled as a function of discrete time intervals τ. For this purpose, following the treatment of Dankwerts it is convenient to define an average flux J_τ as

$$J_\tau = Q/\tau = n_g HRT[(D_l/\tau\pi)^{1/2} \exp(-k\tau) + \{(D_l k)^{1/2} + 1/(2\tau)\ (D_l/k)^{1/2}\} \operatorname{erf}(k\tau)^{1/2}] \quad (4)$$

The uptake coefficient (γ_{meas}) is related to eq 4 via $J_\tau = n_g(c/4)\gamma_{meas}$, where c is the average molecular speed.

Equations 2–4 are applicable when the liquid is stationary with respect to the gas. This is not the case in our experiment. The gas bubble and the surrounding liquid do not move at the same speed. Analysis of the experimental results indicates that the equations have to be modified to take into account the slip between the gas in the bubble and the nearby liquid in the flow tube and eddy current convective transport within the liquid induced by the slip. Modeling of the gas uptake also has to consider species desorption from the liquid both in the flow tube and in the trough and uptake limitation due to gas-phase transport.

In laminar flow, the velocity of the liquid at the wall is zero, resulting in a velocity gradient across a flow tube. Therefore, there is always a slip between the gas in the bubble and part of the liquid in the flow tube, such that some of the liquid is always moving slower than the bubble. The effect of slip on the uptake process is visualized as follows: During the transport along the flow tube, the bubble continually sheds some of the liquid surrounding it. The liquid that is left behind contains solvated species that have entered the liquid from the gas phase. The liquid that has been shed then mixes with the liquid upstream, behind the bubble, resulting in a dilution of the solvated species. The diluted, solvated species left behind then becomes part of the liquid medium encountered by the next bubble. The slip as described, enhances uptake of the gas-phase species in the bubble because the new liquid encountered by the bubble is further from saturation than the liquid that was shed.

We associate the slip with a characteristic time τ (as in eqs 3 and 4) interpreted as the time required for the liquid to slip a significant part of the bubble length. This parameter is to be determined by fitting the experimental data. To model this effect, we assume that the bubble is advanced from the injector to the point of exit from the flow tube in time steps of τ. At any point along the flow tube, the gas–liquid interaction time (t') is given by $t' = n\tau$ where n is the number of steps to that point. The gas uptake from the bubble (Δn_g) during the time interval τ is computed using eq 4. The amount of gas Δn_g is then added to the liquid to compute the new liquid-phase density (n_l) of the species. Modeling of the experimental data shows that the slip time τ is inversely proportional to the bubble velocity v_b. That is $\tau = C_1/v_b$. As shown below, C_1 defines the enhanced uptake due to this effect.

Non-reactive Species. To obtain a best fit value for τ, we first model the uptake of non-reactive species ($k = 0$). The net amount of gas entering the liquid phase at time t' during a period τ is

$$\Delta n_g(t') = J_\tau(t')(S_b/V_b)\tau = [n_g(t')HRT - n_l(t')]2(D_l/\pi\tau)^{1/2}\ (S_b/V_b)\tau \quad (5)$$

Here S_b and V_b are respectively the effective surface area and volume of the bubble. The second term in the brackets takes into account the return of solvated species from liquid to gas phase. The sides of the bubble are in contact with the flow tube and are to some extent isolated from the bulk liquid. Therefore, the ratio (S_b/V_b) is expected to be smaller than the geometric surface to volume ratio $(S_b/V_b)_{geo}$. That is $(S_b/V_b) = C_2(S_b/V_b)_{geo}$, with C_2 to be determined by fitting the experimental data.

The species density in the bubble at the next step Δt is

$$n_g(t' + \tau) = n_g(t') - \Delta n_g(t') \quad (6)$$

Correspondingly, the species density in the liquid at that point is

$$n_l(t' + \tau) = [n_l(t') + \Delta n_g(t')(V_b/V_l)] \quad (7)$$

Here V_l is the volume of the liquid associated with each bubble. (The ratio V_b/V_l is the measured bubble-volume to liquid-volume ratio in the flow tube.)

In this way the density of the trace species n_g is followed from $t' = 0$ to $t' = t$ with the initial condition $n_g(0) = n_0$, the initial gas-phase species density, and $n_l(0) = 0$. (t is the full travel time of the bubble from the injector to the exit from the flow tube.)

The uptake data make it evident that the model, as it stands, underestimates the detected gas-phase species density. This underestimate is attributed to species desorption as the liquid flows out of the flow tube into the reservoir. In this exit region over the reservoir, the liquid as it leaves the flow tube encounters a region of lower gas-phase species density, and consequently part of the solvated species desorbs. Simple equilibrium considerations show that the resulting increase in the species density, n_g', is of the form

$$n_g' = n_l(t)C_3[1 + HRTC_4]^{-1} \quad (8)$$

Here C_3 and C_4 are relevant effective gas to liquid volume ratios to be determined by fitting the experimental data.

The final detected gas-phase species density, $[n_g(t)]_F$ is

$$[n_g(t)]_F = n_g(t) + n_g' \quad (9)$$

Reactive Species. As a first attempt at modeling the effect of irreversible liquid-phase reaction on gas uptake, we simply include the reactive terms as shown in eq 4 in the expression for Δn_g in eq 5. Furthermore, eq 7 is multiplied by $\exp(-k\tau)$, and eq 8 is multiplied by $\exp(-kC_5)$; where C_5 is the effective residence time as the exiting liquid mixes into the reservoir.

The results of reactive uptake measurements show that modeling with these first-order modifications alone underestimates the reactive uptake. This is not unexpected. We note that there is a qualitative difference in the nature of the uptake process for non-reactive and reactive species. In the former case, the species remains solvated in the liquid. In the latter, the species disappears as a result of irreversible chemical reactions. In both cases, the rate of gas uptake is determined by the rate at which the solvated species is removed from the gas–liquid interface. However, eddy currents in the liquid near the gas–liquid interface may preferentially enhance the uptake of reactive compared to non-reactive species. As an example, assume that, in the process of bubble slip through the liquid, small scale eddy currents are setup near the gas–liquid interface. In the case of non-reactive species, such an eddy current will first remove solvated molecules from the interface but then the current will return them back again, resulting in zero net removal of solvated species near the interface. On the other hand, in the case of reactive species, if the reaction rate is sufficiently rapid, the concentration of the solvated species will decrease during the eddy current period. Therefore, a smaller number of trace species will be brought back to the interface than removed from it. In this case, such small scale eddy currents enhance reactive gas uptake. The effect of such an eddy

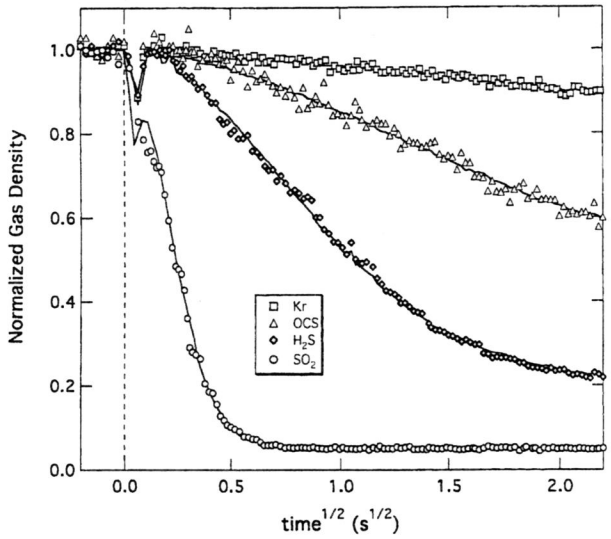

FIGURE 3. Uptake of four non-reactive species, Kr, OCS, H_2S, and SO_2 (the latter two at pH 1 to avoid hydrolysis reaction) at 293 K as a function of square root of gas liquid interaction time ($t^{1/2}$). H varies from 2.83 × 10^{-3} (Kr) to 1.84 (SO_2) M atm^{-1}. Solid line is the computer model fit to the data.

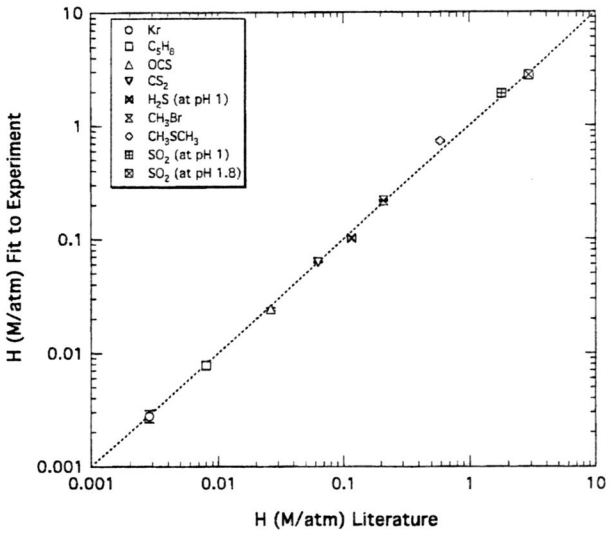

FIGURE 4. Henry's law coefficients at 293 K determined by computer fit to the experimental data versus the literature values. The error bars represent the 2σ standard deviation in the model fitting of the measured uptake as in Figure 3.

current convection on the uptake will certainly be a function of the reaction rate itself.

We have not been successful in formulating a simple picture of convection that would yield a good fit to the reactive uptake data over the full range studied. Therefore, we resorted to seeking a trial function f_D that would provide a fit to the uptake measurements. A good fit to the data with the trial function f_D yielding a modified expression for the flux is

$$J_t' = n_g HRT\{(D_l/\tau\pi)^{1/2} \exp(-k\tau) + [(D_l k)^{1/2} f_D + 1/(2\tau)\,(D_l/k)^{1/2}]\,\mathrm{erf}(k\tau)^{1/2}\} \quad (10)$$

The data are then well fitted with f_D of the form

$$f_D = 1 + C_6 \exp[-HRT(D_l k)^{1/2} C_7] \quad (11)$$

Equation 5 then becomes

$$\Delta n_g(t') = [n_g(t')HRT - n_l(t')]\{(D_l/\pi\tau)^{1/2} \exp(-k\tau) + [(D_l k)^{1/2} f_D + 1/(2\tau)(D_l/k)^{1/2}]\,\mathrm{erf}(k\tau)^{1/2}\}(S_b/V_b)\tau \quad (12)$$

Equation 12 is analogous to eq 4 with the value of τ (i.e., C_1) reflecting convection due to bubble slip, independent of t. Enhanced reactive uptake due to eddy current transport near the interface is represented by f_D.

In the region of very rapid uptake, there is evidence of the uptake rate reaching a limit. We assume that this limitation is due to gas transport to the liquid surface. This effect is taken into account as a resistance to gas flux into the liquid expressed via a parameter C_8 as

$$(J_{net})^{-1} = (J_t')^{-1} + (C_8)^{-1} \quad (13)$$

The parameter C_8 affects uptake only in the region of the very fastest uptakes studied with this apparatus.

Experimental Results

Calibration of the Apparatus. Four parameters are needed to model the uptake of non-reactive species: C_1, C_2, C_3, and C_4. These parameters were obtained by studying the uptake of species with nine known Henry's law coefficients varying over 3 orders of magnitude. As an example of the uptake data, we show in Figure 3 the uptake of four non-reactive species, Kr, OCS, H_2S, and SO_2 at 293 K, the latter two at pH 1 to avoid hydrolysis of the dissolved gas. The normalized density of the gas-phase species is plotted as a function of the square root of the gas–liquid interaction time to emphasize the short time data where the gas uptake rate is largest. Similar data are obtained for the other species. Solid lines in the figure are computer model fits to the data obtained by fixing the Henry's law coefficient at the literature values and using a non-linear least squares fitting routine to determine the values for a subset of the parameters that gives the best simultaneous fit of the model to all data sets. The subset of parameters was changed and the data were refit until the global minimum best fit was found. Using these parameters, the data sets were refit by the model and yielded the final values for the Henry's law coefficients. These were in good agreement (within 8%) with the published values. The discontinuities in the model fits shown in Figure 3 reflect pressure changes as the injector enters deeper into the liquid. These changes are included in the modeling.

TABLE 1. Modeling Parameters at 293 K As Defined in the Text

C_1	0.448 cm	C_5	20.0 s
C_2	0.910	C_6	2.39
C_3	0.121	C_7	0.608 s
C_4	7.24 × 10^{-3}	C_8	19.1 cm^{-2} s^{-1}

In Figure 4 we show Henry's law coefficients as determined by fitting the model to the experimental data plotted versus the literature values. The literature values for the Henry's law coefficients were obtained from Wilhelm et al. (*39*) for Kr, CH_3Br, OCS, SO_2, and H_2S; Mackay et al. (*40*) for 1,4-butadiene (C_5H_8); Aneja and Overton for DMS (*41*); and De Bruyn et al. (*24*) for CS_2. For all species, the liquid-phase diffusion coefficients are calculated using the cubic cell model of Houghton (*42*). Where comparison is possible, this model is in excellent agreement with experimental data. The liquid-phase diffusion coefficients in these experiments ranged from 1.01 to 1.56 × 10^{-5} cm^2/s. The values for the four parameters C_1–C_4 are listed in Table 1. The H values obtained from the modeling of the measured uptake are on the average within 8% of the literature values.

To validate the uptake model for gas-phase species that undergo chemical reactions in the surrounding liquid, a second series of uptake studies was done with ozone and formaldehyde. The following uptake studies were performed: O_3 with Br^-, Fe^{2+}, NO_2^-, OCl^-, I^-, HS^-, and

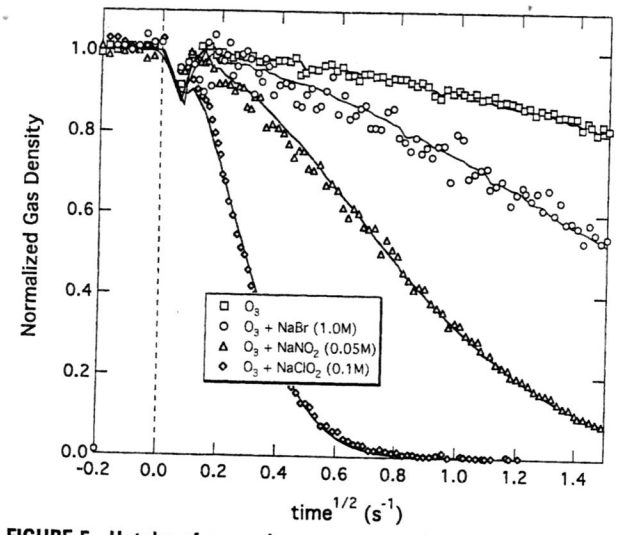

FIGURE 5. Uptake of ozone by pure water with 1.0 M Br^-, 0.05 M NO_2^-, and 0.1 M ClO_2^- at 293 K as a function of square root of gas liquid interaction time ($t^{1/2}$). The reaction rate k varies from 1.13 × 10^2 s^{-1} (Br^-) to 1.54 × 10^5 s^{-1} (ClO_2^-). Solid line is the computer model fit to the data.

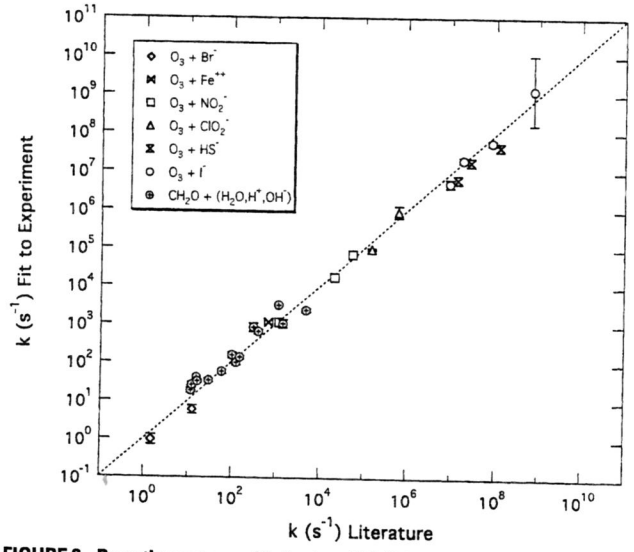

FIGURE 6. Reaction rate coefficients at 293 K determined by computer fit to the experimental data versus the literature values. The error bars represent the 2σ standard deviation in the model fitting of the measured uptake as in Figure 5.

formaldehyde in the pH range 0−11. The H and k values for O_3 are respectively from Kosak-Channing et al. (*43*) and Hiogné et al. (*44*). The Henry's law coefficient for CH_2O is obtained from Betterton and Hoffman (*44*), and the reaction rates for CH_2O are from Bell et al. (*46, 47*) and Valenta (*48*). In these studies, k ranged from about 1 to 10^8 s^{-1}. As an example of reactive uptake, we show in Figure 5 the uptake of ozone by pure water and solutions of 1.0 M Br^-, 0.05 M NO_2^-, and 0.1 M ClO_2^- at 293 K. Here again uptake is plotted as a function of $t^{1/2}$. The effect of the reactive uptake is clearly evident. The solid lines are the model fit to the data.

In all, 30 reactive systems were studied. A global fitting of the uptake data from these studies yielded the additional four parameters needed to define the uptake model. The values for the parameters C_5−C_8 are listed in Table 1. In Figure 6, we show a plot of k as determined by the model fit to the experimental data versus literature values of k. The k values obtained from the modeling of the measured uptake are on the average within 55% of the literature values.

In summary, the eight parameters required to model the uptake were obtained by globally fitting 39 sets of uptake data. The uptake results show that the apparatus in the present configuration can measure Henry's law coefficients (H) for non-reactive species in the range 10^{-3} to 3.0 M/atm. For reactive species (first-order reaction rate k), the apparatus yields $Hk^{1/2}$ values in the range 0.04−150 M atm^{-1} $s^{-1/2}$. If the Henry's law coefficient of a species is known, then first-order reaction rates (k) can be measured in the range 1−10^8 s^{-1}.

The fitting parameters C_1−C_8 were determined at 293 K. Preliminary experiments indicate that these parameters do not change significantly in the range of ±15 K.

Uptake of Gas Phase Formaldehyde

Formaldehyde reacts with water to form methanediol. This reaction is catalyzed by both H^+ and OH^-. Our results were modeled with the acid−base-catalyzed hydrolysis rate constant for formaldehyde, calculated with the methanediol dehydration rate constants for the reverse reaction published by Bell and Evans (*48*) and the equilibrium constant by Valenta (*49*) at 293 K. The pseudo-first-order rate constant k_1 is therefore a function of pH

$$k_1 = 2.09 \times 10^{-1}[H_2O] + 6.14 \times 10^3[H^+] + 3.64 \times 10^6\,[OH^-] \quad (14)$$

The concentration of water is 55.5 M. More recently Los et al. (*48*) measured k_1 at pH greater than 12. In that region their results are in agreement with eq 14.

In two previous studies, we measured the uptake of formaldehyde using our droplet train apparatus. In one study, the uptake of gas-phase formaldehyde by aqueous sulfuric acid (10−70 wt %) and nitric acid (20−54 wt %) was measured as a function of temperature, acid concentration, and gas-droplet contact time (*31*). In the other study, uptake by aqueous droplets in the pH range 1−15 was measured (*32*). In the mid-range region, pH 4−10, the uptake was too small to be detected by the droplet apparatus. The uptake above pH 11 was measurable and was in accord with eq 14. But at low pH, below pH = 2, the uptake was significantly higher than predicted by eq 14.

In the droplet apparatus, the gas−liquid interaction time is short, between 3 and 20 ms. Consequently, the uptake for species of low solubility is small, and uptake specifically associated with the liquid surface, such as the formation of a surface complex or some other surface specific interaction, may be a significant fraction of the total uptake. We suggested that the enhanced uptake observed in the droplet studies was in fact due to an acid-catalyzed surface complex. In the other independent sulfuric acid uptake study, surface-enhanced uptake was also observed.

The newly built horizontal bubble train apparatus provides the opportunity to measure the uptake of gas-phase formaldehyde with greater sensitivity. Since in the bubble apparatus the uptake is much larger, the additional surface uptake should be negligible, and we can test if the uptake is now in accord with bulk phase chemistry as expected. The pseudo-first-order rate constant as a function of pH at 293 K obtained from the uptake measurements is shown in Figure 7. Rates obtained with the droplet apparatus are also shown as solid diamonds. The dashed line is a plot of eq 14. The bubbler data are in reasonably good accord with the bulk phase reaction rates of eq 14. For example, in the pH region 4−8, the rate constant given by eq 14 is 11.6 s^{-1}. Our experimental data yield 15.5 s^{-1}.

Setchenow Saltout Coefficients. It is well-known that the capacity of water to solvate gas-phase species decreases with ionic strength. This can be expressed as a decrease in the Henry's law coefficient. A number of models can be used to express the change in a species activity coefficient with ionic strength. For simple one salt systems, the empirically derived Setchenow relationship is adequate (*50*). In this

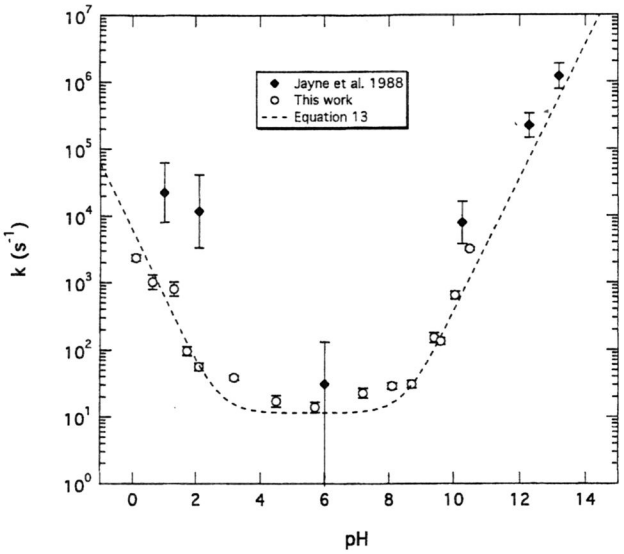

FIGURE 7. Pseudo-first-order rate coefficient for formaldehyde at 293 K as a function of pH. Rates obtained with the droplet apparatus are shown as solid diamonds. The larger rate at low pH measured with the droplet apparatus is suggested to be due to an acid-catalyzed surface interaction. Dashed line is eq 13.

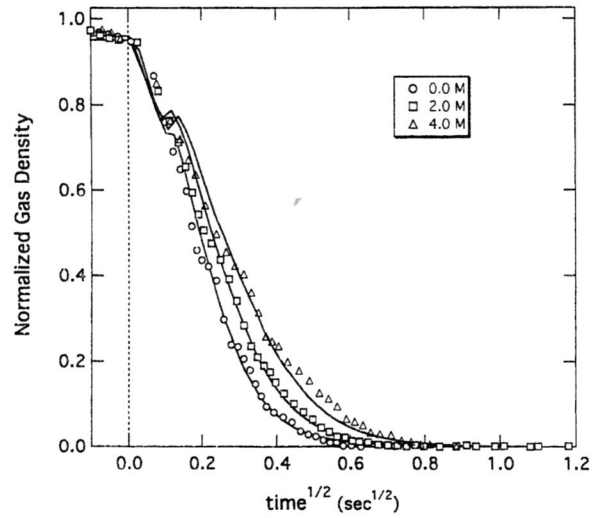

FIGURE 8. Uptake of formaldehyde by pure water, 2.0 M and 4.0 M solutions of NaCl at 293 K as a function of $t^{1/2}$. Due to salting out, uptake rate decreases with increasing NaCl concentration.

formulation, the decrease in the Henry's law coefficient is expressed as

$$\log_{10} H^{o}/H = K_s M \qquad (15)$$

where H^o is the Henry's law coefficient in pure water, M is the molarity of the ionic solution, and K_s is the Setchenow salt out coefficient (in units of M^{-1}).

The salting out effect is clearly evident in Figure 8, which shows the uptake of formaldehyde by pure water, 2.0 M and 4.0 M solutions of NaCl. From such measurements, H as a function of salt concentration can be obtained. Since the uptake of formaldehyde is a function of both H and k, to calculate H, the uptake model must be provided with a value of k as a function of the salt solution activity. We used a value of $k = 15.5\ s^{-1}$, which is our measured value of k in the pH 4–7 region. The activity coefficients were obtained from Pitzer (*49*). In Figure 9, we show a plot of log H/H^o as a function salt concentration for formaldehyde in NaCl solutions. The slope of the plot is $-K_s$. The Setchenow coefficients at 293 K is $K_s = 0.072 \pm 0.004\ M^{-1}$. Setchenow coefficients

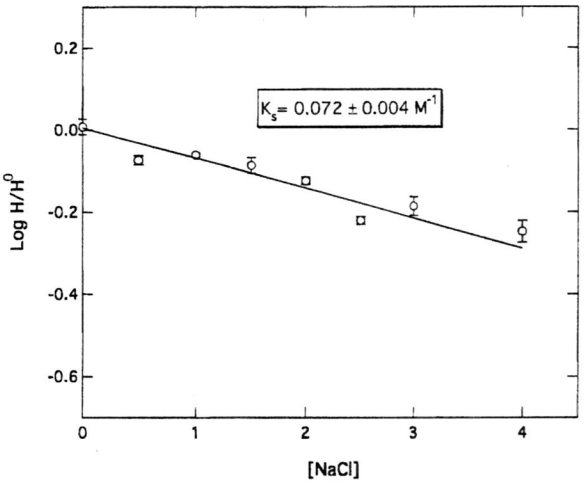

FIGURE 9. Log_{10} (H^o/H) as a function of salt concentration for formaldehyde in NaCl solutions. Setchenow coefficient K_s at 293 K is obtained from the slope of the least squares fit line.

are not expected to exhibit a significant temperature dependence over the range 278–298 K. For example, Barret et al. (*51*) observed a less than 1% change in the ratio H^o/H for H_2S in NaCl in the temperature range 298–348 K.

Acknowledgments

Funding was provided by National Science Foundation Grants ATM-93-10407 and ATM-96-32599, by U.S. Environmental Protection Agency Grant R-821256-01-0, by Department of Energy Grants DE-FG02-91ER61208 and DE-FG02-94ER61854, and by NASA Grant NAS-5-3263.

Literature Cited

(1) Graedel, T. E.; Goldberg, K. I. *J. Geophys. Res.* **1983**, *88*, 10865.
(2) Heikes, B. G.; Thompson, A. M. *J. Geophys. Res.* **1983**, *88*, 10883.
(3) Chameides, W. L. *J. Geophys. Res.* **1984**, *89*, 4739.
(4) Finlayson-Pitts, B. J.; Pitts, J. N. *Atmospheric Chemistry*; John Wiley and Sons: New York, 1986.
(5) Schwartz, S. E. *J. Geophys. Res.* **1984**, *89*, 11589.
(6) Jacob, D. J. *J. Geophys. Res.* **1986**, *91*, 9807.
(7) Coakley, J. A., Jr.; Bernstein, R. L.; Durkey, P. A. *Science* **1987**, *237*, 1020.
(8) Charlson, R. J.; Lovelock, J. E.; Andreae, M. O.; Warren, S. G. *Nature* **1987**, *326*, 655.
(9) Lelieveld, J.; Heintzenberg, J. *Science* **1992**, *258*, 117.
(10) Jonson, E. J.; Isaksen, S. A. *J. Atmos. Chem.* **1993**, *16*, 99.
(11) Solomon, S. *Rev. Geophys.* **1988**, *26*, 131.
(12) Wofsy, S. C.; Molina, M. H.; Salawitch, R. J.; Fox, L. E.; McElroy, M. B. *J. Geophys. Res.* **1988**, *93*, 2442.
(13) Rodriguez, J. M. *Science* **1994**, *261*, 1128.
(14) Abbatt, J. P. D.; Molina, M. J. *Annu. Rev. Energy Environ.* **1993**, *18*, 1.
(15) Huntzicker, J. J.; Cary, R. A.; Ling, C.-S. *Environ. Sci. Technol.* **1980**, *14*, 819.
(16) McMurry, P. H.; Tahano, H.; Anderson, G. R. *Environ. Sci. Technol.* **1983**, *17*, 347.
(17) Golden, D. M.; Spokes, G. N.; Benson, S. W. *Angew. Chem. Int.* **1973**, *12*, 53.
(18) Utter, R. G.; Burkholder, J. B.; Howard, C. J.; Ravishankara, A. R. *J. Phys. Chem.* **1992**, *96*, 49.
(19) Gardner, J. A.; Watson, L. R.; Adewuyi, Y. G.; Davidovits, P.; Zahniser, M. S.; Worsnop D. R.; Kolb, C. E. *J. Geophys. Res.* **1987**, *92*, 10887.
(20) Worsnop, D. R.; Zahniser, M. S.; Kolb, C. E.; Gardner, J. A.; Watson, L. R.; Van Doren, J. M.; Jayne, J. T.; Davidovits, P. *J. Phys. Chem.* **1989**, *93*, 1159.
(21) George, Ch.; Lagrange, J.; Lagrange, Ph.; Mirabel, Ph.; Pallares C.; Ponche, J. L. *J. Geophys. Res.* **1994**, *99*, 1255.
(22) Kolb, C. E.; Worsnop, D. R.; Zahniser, M. S.; Davidovits, P.; Keyser, L. F.; Leu, M.-T.; Molina, M. J.; Hanson, D. R.; Ravishankara, A. R.; Williams, L. R.; Tolbert, M. A. Laboratory Studies of Atmospheric Heterogeneous Chemistry In *Progress and Problems in Atmospheric Chemistry*; Barker, J. R., Ed.; *Advanced Series in Physical Chemistry*; World Scientific Publishing Co.: Singapore, 1995; pp 771–921.

(23) Shorter, J. A.; De Bruyn, W. J.; Hu, J. H.; Swartz, E.; Davidovits, P.; Worsnop, D. R.; Zahniser, M. S.; Kolb, C. E. *Environ. Sci. Technol.* **1995**, *29*, 1171.
(24) De Bruyn, W. J.; Swartz, E.; Shorter, J. A.; Davidovits, P.; Worsnop, D. R.; Zahniser, M. S.; Kolb C. E. *J. Geophys Res.* **1995**, *100* (D4), 7,425.
(25) Baugh, J.; Ray, W.; Black, F. *Atmos. Environ.* **1987**, *21*, 2077.
(26) See, for example, Tichenor, B. A.; Mason, M. A. *J. Air Pollut. Control Assoc.* **1988**, *38*, 264.
(27) Calvert, J. C.; Madronich, S. *J. Geophys. Res.* **1987**, *92*, 2211.
(28) See, for example, Russell, A.; Milford, J.; Bergin, M. S.; McNair, L.; Yang, Y.; Stockwell, W. R.; Croes, B. *Science* **1995**, *269*, 491.
(29) See, for example, Rao, X.; Collett, J. L., Jr. *Environ. Sci. Technol.* **1995**, *29*, 1023.
(30) See, for example, Jacob, D. J. *J. Geophys. Res.* **1986**, *91*, 9807.
(31) Jayne, J. T.; Worsnop, D. R.; Kolb. C. E. ; Swartz, E.; Davidovits, P. *J. Phys. Chem.* **1996**, *100* (19), 8015.
(32) Jayne, J. T.; Duan, S. X.; Davidovits, P.; Worsnop, D. R.; Zahniser, M. S.; Kolb. C. E. *J. Phys. Chem.* **1992**, *96*, 5452.
(33) Davidson, J. F.; Schuler, B. O. G. *Trans. Inst. Chem. Eng.* **1960**, *38*, 335.
(34) Kupferberg, A.; Jameson, G. J. *Trans. Inst. Chem. Eng.* **1969**, *47*, 241.
(35) Davidson, L.; Amick, E. H. *AIChE J.* **1956**, *2*, 337.
(36) Hayes, W. B.; Hardy, B. W.; Holland, C. D. *AIChE J.* **1959**, *5*, 319.
(37) Marmur A.; Rubin, E. C. *Eng. Sci.* **1976**, *31*, 453.
(38) Danckwerts, P. V. *Trans. Faraday Soc.* **1950**, *46*, 300; *Trans. Faraday Soc.* **1951**, *47*, 1014.
(39) Wilhelm, E.; Battino, R.; Wilcock, R. J. *Chem. Rev.* **1977**, *77*, 219.
(40) Mackey, D.; Shiu W. Y. *J. Phys. Chem. Ref. Data* **1981**, *10* (4), 1175.
(41) Aneja, V. P.; Overton, H. J. *Chem. Eng. Commun.* **1990**, *98*, 199.
(42) Houghton G. *J. Phys. Chem.* **1964**, *40* (4), 1628.
(43) Kosak-Channing, L. F.; Helz, G. R. *Environ. Sci. Technol.* **1983**, *17*, 154.
(44) Hoigné, J.; Bader, H.; Haag, W. R.; Staehelin, J. *Water Res.* **1985**, *19*, 993.
(45) Betterton, E. A.; Hoffman, M. P. *Environ. Sci. Technol.* **1988**, *22*, 1415.
(46) Bell, A. P. *Adv. Phys. Org. Chem.* **1966**, *4*, 1.
(47) Bell, R. P.; Evans, P. G. *Proc. R. Soc. A*, **1966**, *291*, 297.
(48) Valenta, P. *Collect. Czech. Chem. Commun.* **1960**, *25*, 853.
(49) Los, J. M.; Brinkman, A. A. A.; Wetsema, B. J. C. *Electroanal. Chem. Interface Electrochem.* **1974**, *56*, 187.
(50) Clegg, S. L.; Whitfield, M. In *Activity Coefficients in Electrolyte Solutions*, Pitzer, K. S., Ed.; CRC Press: Boca Raton, FL, 2nd ed.; 1991; pp 279–434.
(51) Barret, T. J.; Anderson, G. M.; Lugowski, J. *Geochim. Cosmochim. Acta* **1988**, *52*, 807.

Received for review January 21, 1997. Revised manuscript received May 1, 1997. Accepted May 5, 1997.[⊗]

ES970042W

[⊗] Abstract published in *Advance ACS Abstracts,* July 1, 1997.